Microstructure analysis at the interface of Er decorated Ge nanocrystals in SiO_2

A. Kanjilal,[1,*] S. Gemming,[1] L. Rebohle,[1] A. Muecklich,[1] T. Gemming,[2] M. Voelskow,[1] W. Skorupa,[1] and M. Helm[1]
[1]*Institute of Ion Beam Physics and Materials Research, Forschungszentrum Dresden-Rossendorf, PO Box 51 01 19, D-01314 Dresden, Germany*
[2]*Institute for Complex Materials, IFW Dresden, PO Box 27 01 16, D-01171 Dresden, Germany*

(Received 16 December 2010; published 8 March 2011)

Using scanning transmission electron microscopy and aberration-corrected high-resolution transmission electron microscopy the existence of Er around Ge nanocrystals (NCs) is established. In fact, Ge NCs with Er-rich graded interfaces are proposed experimentally and validated by theoretical modeling using a *supercell* structure that consists of compounds determined by x-ray diffraction. The local electronic structure of the proposed interface geometry is found to be in accordance with the hypothesis behind the inverse energy transfer process from the Er^{3+} to Ge related oxygen-deficiency centers.

DOI: 10.1103/PhysRevB.83.113302 PACS number(s): 78.67.Bf, 71.20.Eh, 79.20.Uv, 85.60.Jb

Energy saving light emitters (LEs), especially the production of economic white and bright light-emitting sources based on blue-violet devices enriched with yellow phosphors is a frontier field of research.[1] Successful fabrication of LEs according to Haitz's law[1] relies on the elaborate manufacturing techniques and complex design of LEs. Although semiconductor nanocrystals (NCs)[2] and/or rare-earth ions[3,4] in a metal-oxide semiconductor (MOS) structure have shown their potential to develop efficient LEs, they have yet to reach the ultimate goal. In parallel, Si nanoparticles have been used as *sensitizers* in Er-doped SiO_2 for achieving an enhanced 1.53-μm Er photoluminescence[5–8] or electroluminescence (EL).[9] Recently, alternatives based on Ge nanoparticles in Er-doped MOSLEs have also been demonstrated. Such MOSLEs provide an enhanced 400-nm EL at the expense of the 1.53-μm Er emission[10–12] and has been explained in the framework of an *inverse energy-transfer* process from the Er^{3+} to the Ge related oxygen-deficiency centers (GeODCs).[10] Note that the 400-nm EL is associated with the first-triplet to the ground-singlet ($T_1 \rightarrow S_0$) transition in GeODCs,[10] whereas the intra-$4f^4 I_{13/2} \rightarrow {}^4I_{15/2}$ transition in Er^{3+} leads to the 1.53-μm Er emission.[13]

Although the existence of Er^{3+} in the vicinity of Ge NCs has been accepted previously to explain the observed EL,[10] detailed microstructure analysis at the NC/SiO_2 interface has not been reported yet. Here, we show the formation of an Er-rich graded interface at the NC-SiO_2 boundary using a combined experimental and theoretical approach. Initially, a theoretical modeling has been developed using a *supercell* structure that consists of compounds determined by x-ray diffraction.[12] In fact, the first principle calculation of the proposed interface geometry gives the local electronic structure, which is in agreement with the hypothesis behind the inverse energy-transfer process from the Er^{3+} to the GeODCs.[10] The Er-rich graded interface model is also corroborated by x-ray structure determination,[12] scanning transmission electron microscopy (STEM),[14] and aberration-corrected high-resolution transmission electron microscopy (HRTEM).[15]

The standard metal-oxide-semiconductor structures were fabricated by local-oxidation of Si (LOCOS) technology with a 200-nm-thick thermally grown SiO_2 layer on *n*-type Si(100) wafers. Initially, 130-keV Ge ions were implanted into the SiO_2 layer, with a maximum concentration in the range of 3.5%–11.1% at $R_p \sim 112$ nm as derived from the SRIM-2006 calculations.[16] The samples were annealed at 950 °C in a nitrogen atmosphere for 60 min. Subsequently, 250-keV Er ions were implanted with a maximum concentration lying in the range of 0.3%–1.4% at $R_p \sim 115$ nm, followed by annealing at 900 °C for 30 min in a nitrogen ambiance. A 100-nm-thick Si-oxynitride (SiON) layer was deposited on top of the LOCOS structure, followed by the growth of semi-transparent indium-tin-oxide (ITO) and aluminum contacts on the front and rear surfaces, respectively. The ITO layer was patterned by optical lithography to prepare circular electrodes (diameter ~300 μm). Depth profiles of the implanted elements were verified by performing Rutherford-backscattering spectrometry (RBS) using a 1.4-MeV He^+ beam. High angle annular dark-field (HAADF)-STEM, HRTEM, energy-filtered TEM (EFTEM), energy-dispersive x-ray spectroscopy (EDS), and electron energy-loss spectroscopy (EELS) measurements were performed in cross-sectional geometry using a FEI-Titan 80-300 S/TEM instrument operating at 300 keV.

On the other hand, density-functional calculations (Fig. 1) were performed with the program package ABINIT,[17] employing the generalized gradient approximation provided by the PBE exchange and correlation functions[18] and the PAW package.[19] An $8 \times 8 \times 4$ Monkhorst-Pack mesh, a plane-wave energy cutoff of 551 eV, and a parameter $U = 7.94$ eV (Ref. 20) for the localized states at the Er centers were applied; the density of states (DOS) curve in Fig. 1(d) is broadened with a Gaussian smearing of 0.125 eV, while the isodensity contours depicted in Fig. 1(c) correspond to 10% of the maximum density of the corresponding state.

Considering the importance of Er^{3+} around Ge NCs in Er-doped Ge-rich MOSLEs,[10] a model structure at the NC/SiO_2 interface is proposed for evaluating the electronic properties. The presently employed supercell structure (Fig. 1) was derived from earlier x-ray structure investigations,[12] which revealed traces of Er-pyrogermanate ($Er_2Ge_2O_7$) as the secondary phase in Ge-rich SiO_2 when co-doped with 0.5% Er and annealed at 1100 °C for 30 min. The formation energies $H_f(GeO_x) \ll H_f(SiO_2) < H_f(Er_2Ge_2O_7)$ and $H_f(Er_2Si_2O_7) < H_f(Er_2O_3)$ suggest a thermodynamic driving force for the development of an Er-rich layer as a surfactant

 ©2011 American Physical Society

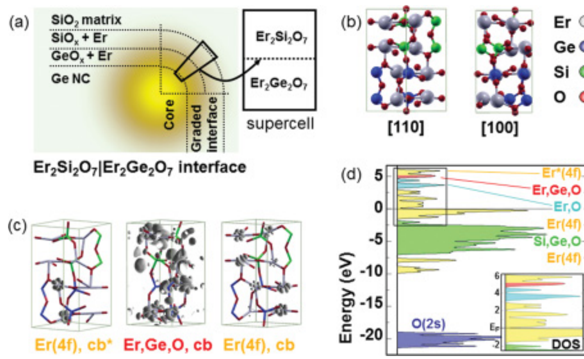

FIG. 1. (Color online) (a) Schematic view of the Er-rich graded interface between Ge NC core and surrounding SiO_2, showing the setup of the supercell for DFT calculation. (b) Model supercell structure consisting of $Er_2Si_2O_7(001)$ and $Er_2Ge_2O_7(001)$ layers. (c) Spatial extension of the conduction band (cb) states, representing high-lying Er(4*f*) cb* states localized at Er in the Ge-rich layer, occurrence of mixed (Er,Ge,O) cb states at lower energy and lower lying Er(4*f*) cb states. (d) Calculated DOS (E_F set to zero) for the supercell depicted in (b) giving the relative energy alignment of the Er-containing cb states and the occupied valence states; colors (different gray tones) denote the character of the peak obtained from a spatial decomposition of the DOS. The inset gives a magnified view of the DOS in the vicinity of E_F.

to lower the interfacial energy between Ge NCs and the surrounding SiO_2 matrix. Moreover, based on previous understanding of the observed EL behavior,[10–12] a graded interface with Er-rich pyrogermanate and pyrosilicate layers at the NC-SiO_2 boundary is considered here [Fig. 1(a)], where the model structure is a mixture of $Er_2Si_2O_7(001)$ and $Er_2Ge_2O_7(001)$ layers as exhibited in Fig. 1(b). This choice reflects both the x-ray structure investigations and the decreasing formation energy of silicon, erbium, and germanium oxides. As the lattice parameters of the parent compounds differ by about 7%, optimization of the cell yields averaged supercell lattice parameters. The coordination numbers and the O arrangements around Er, Si, and Ge sites are, however, maintained during relaxation, and do not affect the crystal-field splitting.

To visualize the observed EL behavior,[10] typical conduction-band states of the proposed structure [Fig. 1(b)] are depicted in Fig. 1(c) along with the corresponding DOS [see Fig. 1(d)]. A small band gap of $\sim$0.22 eV [inset of Fig. 1(d)] separates the occupied and unoccupied Er 4*f* states around the Fermi level E_F (set to 0 eV). Further below, the valence band consists of Si-O and Ge-O bonding states, followed by Er 4*f* [between -7.5 and -10 eV, similar to ErAs (Ref. 20)] and O 2*s* states (around -20 eV). The Er 4*f* states at the conduction-band edge are followed by Er- and O-derived states

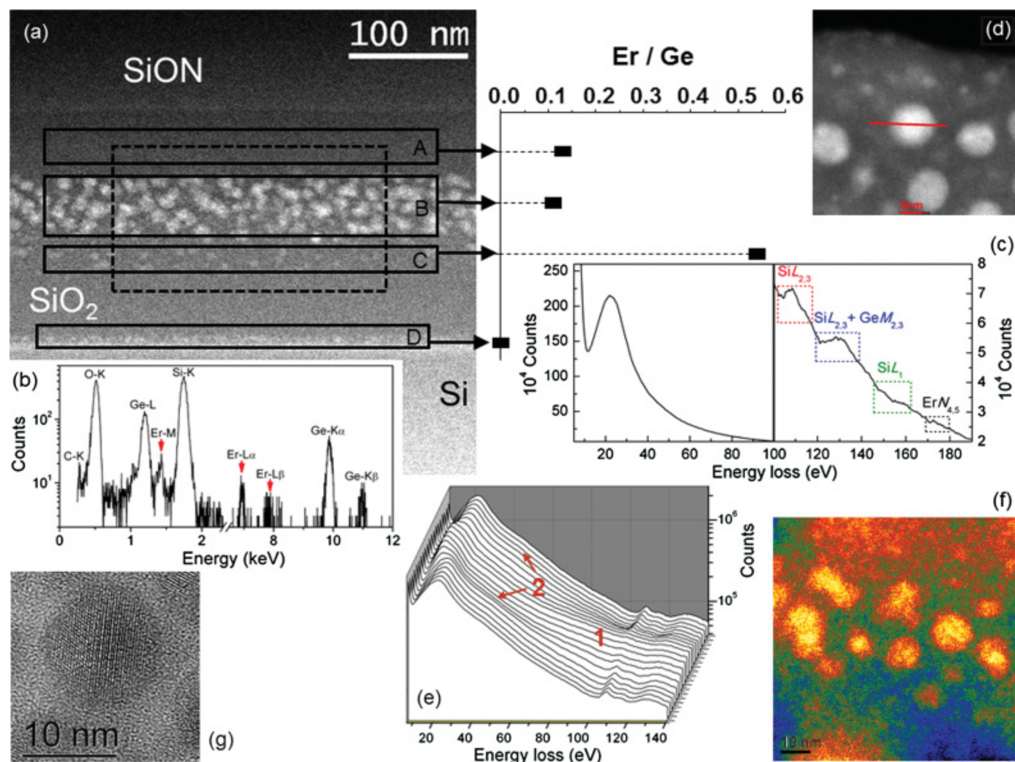

FIG. 2. (Color online) (a) Low magnification HAADF-STEM image, showing the distribution of Ge nanoparticles in SiO_2; the intensity ratio of the Er-*L* and Ge-*K* edges in regions of A, B, C, and D is shown in the adjacent plot. (b) and (c) display the EDS and EELS profiles, respectively, taken from the region indicated by a dashed rectangle in (a). (d) High-resolution HAADF-STEM image shows the formation of Ge nanoclusters with sizes in the range 7–10 nm (white contrast), while the small features below 2 nm are mostly Si nanoparticles. The trace [shown in (d)] represents the location along which a sequence of EELS profiles was recorded where a three-dimensional view of the recorded EELS profiles is exhibited in (e). Bands marked by "1" and "2" in (e) are associated with Ge and Er. (f) Bright region represents the high Ge content in the acquired EFTEM image at the Ge $M_{4,5}$ edge. (g) HRTEM image confirms the formation of Ge NCs, while such a typical Ge NC is screened from the surrounding SiO_2 by a dark-gray patch. The scale bars in (d) and (f) are 5 and 10 nm, respectively.

and the delocalized (Er,Ge,O) states, which couple empty Ge *p* and *d* states with Er *f* states via O bridges. As shown by Pourovskii *et al.*,[20] a quantitative calculation of the Er multiplet structure is best achieved beyond the independent particle picture of the density-functional theory (DFT), but the qualitative DOS features are also reproduced well by the DFT. In fact, the occurrence of delocalized (Er,Ge,O) states within the localized unoccupied Er 4*f* manifold is in agreement with the hypothesis behind the inverse energy-transfer process from the Er^{3+} to the GeODCs, and so justifies the experimental evidence of the enhanced blue-violet EL.[10]

For detailed microstructural analysis, nanoparticles have been characterized by HRTEM, EFTEM, and HAADF-STEM in combination with EDS and EELS. A cross-sectional HAADF-STEM image of a sample containing 7.4% Ge and 0.8% Er is displayed in Fig. 2(a), showing an overall distribution of Ge nanoparticles (bright) in SiO_2. Note that no significant change is observed in Ge distribution after Er doping. A rectangular (dashed) box in Fig. 2(a) indicates the location from where the EDS and EELS profiles were recorded. The presence of elements such as Er and Ge along with Si and O is verified by EDS [Fig. 2(b)]. By taking the EDS in regions of A, B, C, and D, the intensity ratio of the Er-*L* and Ge-*K* edges was measured [Fig. 2(a)] to have the depth profile of the implanted species. On the other hand, the Ge $M_{4,5}$ edge at 28.7 eV (Refs. 21 and 22) and the Er $O_{2,3}$ edge at 29.4 eV (Refs. 21 and 23) are almost invisible in the recorded EELS profiles [Fig. 2(c)] due to the presence of the strong SiO_2 plasmon at ∼22 eV (Ref. 21) in the lower energy window (5–100 eV). In addition, the presence of the extended Si $L_{2,3}$ edge of SiO_2 near the Ge $M_{2,3}$ edge at ∼125 eV does not give a clear signature of the presence of Ge [right panel, Fig. 2(c)]. However, by measuring a sequence of EELS across a Ge nanoparticle [along the trace in Fig. 2(d)], one can find (i) a gradual transition from the plasmon of SiO_2 (22 eV) to Ge nanocluster (17 eV) (Ref. 24) and back to SiO_2, and (ii) the evolution of a broad tail (60–120 eV) of Ge (Ref. 25) from the cluster (marked by "1") in Fig. 2(e). Although the bulk plasmons are dominant in Fig. 2(e), an additional broad peak (marked by "2") in the range 30–45 eV can also be detected near the edges of the Ge nanoparticle. The origin of such a feature is possibly associated with the $5p \rightarrow 4d$ transitions in Er.[26] We were also able to map the Ge [Fig. 2(f)] using background subtracted EFTEM at the energy loss of Ge-$M_{4,5}$. Additionally, the HRTEM image shows the formation of Ge NCs where the lattice fringes are separated from the amorphous SiO_2 (light gray) matrix by an almost 1-nm-thick amorphous patch (dark gray) [see Fig. 2(g)]. As the atomic weight of Er is about 2.3 times higher than that of Ge, the dark-gray contrast across the crystalline Ge core can be tentatively attributed to the existence of an Er-rich zone, in agreement with the EELS measurements.

In HAADF-STEM imaging the intensity of an atom site depends on the atomic number *Z* as roughly $Z^{1.7}$ (Ref. 27). Judging from the ratio of the *Z* values, the contrast of Ge should be about 3.6 times weaker than that of Er in the ideal case. However, the relative intensity is certainly different in amorphous SiO_2 [see Figs. 2(a) and 2(d)], though EDS on an individual Ge nanoparticle reveals the existence of Er (not shown). In order to assess this effect, the *Z*-contrast intensity of the observed Ge nanoparticle was simulated by the weighted sum of the $Z^{1.7}$ of the atoms in a unit volume under the assumptions of (i) atomically unresolved imaging in amorphous SiO_2, and (ii) out of zone-axis conditions for the clusters. The *Z*-contrast simulations were carried out for Ge NCs embedded in a 30-nm-thick SiO_2 layer and a STEM beam size of 0.5 nm. Simulated HAADF images of a Ge NC (10 nm diameter) with a 1-nm-thick $Er_2Ge_2O_7$ interface layer, a Ge NC (8 nm diameter) with a 1-nm-thick Er shell, and a pure Ge NC (10 nm diameter) are shown in Figs. 3(a)–3(c). Figure 3(d) shows a quantitative comparison of the intensity profiles across the center of all three simulated images shown in Figs. 3(a)–3(c). All models lead to bright images, which are almost identical in size. While the pure Er is visible in the image as a bright ring, the $Er_2Ge_2O_7$ interface layer can hardly be detected when it is compared to Ge NC alone. However, close inspection reveals that the intensity reduces gradually across the cluster boundaries in the presence of the $Er_2Ge_2O_7$ interface layer. Comparison with experimental images [Figs. 2(a) and 2(d)] excludes the existence of a pure Er shell around Ge NCs as the experiments do not show a bright ring around the particles. In this scenario, the $Er_2Ge_2O_7$ interface layer is consistent with the experimental HAADF-STEM images. Considering the aforementioned experimental results and the *Z*-contrast simulations into account we argue that Ge NCs with Er-rich graded interfaces are formed in SiO_2, which is also in good agreement with our theoretical understanding.

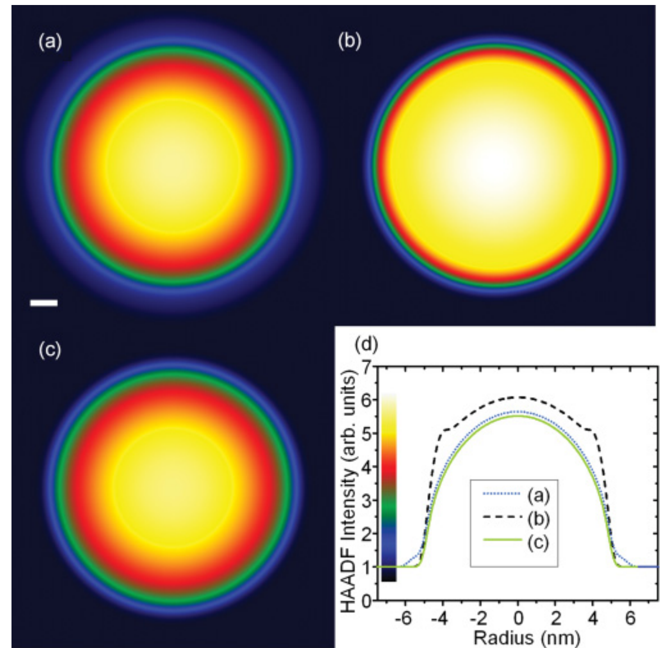

FIG. 3. (Color online) *Z*-contrast simulations were performed for (a) a Ge NC (10 nm diameter) with 1-nm-thick $Er_2Ge_2O_7$ interface layer, (b) a Ge NC (8 nm diameter) with 1-nm-thick Er covering, and (c) a pure Ge NC (10 nm diameter). (d) A quantitative comparison of the intensity profiles across the center of all three simulations shown in (a)–(c). In all cases the particles were embedded in a 30-nm-thick amorphous SiO_2 matrix and were imaged using a 0.5-nm electron probe. The color scale (grayscale) is embedded in panel (d) where the length of the scale bar in (a) is 1 nm.

Using RBS,[12] we also found that the Er atoms are mainly situated in the regions B and C in Fig. 2(a). Assuming the formation of graded interface, the Er/Ge ratio of $\sim$0.1 in region B implies that most of the Ge NCs with sizes in the range of 5–10 nm are partially covered by an Er-rich phase. On the other hand, the Er/Ge ratio has increased to $\sim$0.5 in region C, indicating that the Er-rich phases are more pronounced in this region with Ge NCs below 5 nm in size and are possibly able to screen Ge NCs from the surrounding SiO_2.

In summary, we present the formation of an Er-rich graded interface at the Ge NC-SiO_2 boundary using a combined theoretical and experimental approach. Initially, a theoretical modeling is developed using a supercell structure at the NC/SiO_2 interface that consists of compounds determined by x-ray diffraction. The first-principles calculation of the proposed interface geometry gives the local electronic structure where the results are in accordance with the hypothesis behind the inverse energy-transfer process from the Er^{3+} to the GeODCs. The existence of Er, especially the Er-rich graded interface at the NC-SiO_2 boundary, has been explored by investigating the HRTEM, EFTEM, and HAADF-STEM in combination with EDS and EELS in the microstructure level. Finally, the experimentally observed HAADF-STEM images have been assessed by the *Z*-contrast simulations, which confirm the presence of Er composites and the graded structure at the NC/SiO_2 interface.

We thank the Rossendorf Implantation Group for ion implantation and H. Felsmann, C. Neisser, and G. Schnabel for their careful semiconductor preparation work. This work was supported by the Alexander von Humboldt Foundation.

*akanjilal@purdue.edu

[1]S. Pimputkar, J. S. Speck, S. P. DenBaars, and S. Nakamura, Nature Photon. **3**, 180 (2009).

[2]R. J. Walters, G. I. Bourianoff, and H. A. Atwater, Nature Mater. **4**, 143 (2005).

[3]A. Kanjilal, L. Rebohle, W. Skorupa, and M. Helm, Appl. Phys. Lett. **94**, 101916 (2009).

[4]L. Rebohle, J. Lehmann, S. Prucnal, A. Kanjilal, A. Nazarov, I. Tyagulskii, W. Skorupa, and M. Helm, Appl. Phys. Lett. **93**, 071908 (2008).

[5]D. Timmerman, I. Izeddin, P. Stallinga, I. N. Yassievich, and T. Gregorkiewicz, Nature Photon. **2**, 105 (2008).

[6]B. Garrido, C. García, S.-Y. Seo, P. Pellegrino, D. Navarro-Urrios, N. Daldosso, L. Pavesi, F. Gourbilleau, and R. Rizk, Phys. Rev. B **76**, 245308 (2007).

[7]K. Imakita, M. Fujii, and S. Hayashi, Phys. Rev. B **71**, 193301 (2005).

[8]F. Priolo, C. D. Presti, G. Franzò, A. Irrera, I. Crupi, I. F. Iacona, G. Di Stefano, A. Piana, D. Sanfilippo, and P. G. Fallica, Phys. Rev. B **73**, 113302 (2006).

[9]K. Sun, W. J. Xu, B. Zhang, L. P. You, G. Z. Ran, and G. G. Qin, Nanotechnology **19**, 105708 (2008).

[10]A. Kanjilal, L. Rebohle, M. Voelskow, W. Skorupa, and M. Helm, Appl. Phys. Lett. **94**, 051903 (2009).

[11]A. Kanjilal, L. Rebohle, M. Voelskow, W. Skorupa, and M. Helm, J. Appl. Phys. **106**, 026104 (2009).

[12]A. Kanjilal, L. Rebohle, N. K. Baddela, S. Zhou, M. Voelskow, W. Skorupa, and M. Helm, Phys. Rev. B **79**, 161302(R) (2009).

[13]G. H. Dieke, *Spectra and Energy Levels of Rare Earth Ions in Crystals* (Interscience, New York, 1968), Chap. 13.

[14]P. E. Batson, Nature (London) **366**, 727 (1993); U. Kaiser, D. A. Muller, J. L. Grazul, A. Chuvilin, and M. Kawasaki, Nat. Mater. **1**, 102 (2002).

[15]K. W. Urban, Science **321**, 506 (2008).

[16]J. F. Ziegler and J. P. Biersack, *SRIM-2006.02*, [http://www.srim.org].

[17]X. Gonze, J.-M. Beuken, R. Caracas, F. Detraux, M. Fuchs, G.-M. Rignanese, L. Sindic, M. Verstraete, G. Zerah, F. Jollet, M. Torrent, A. Roy, M. Mikami, Ph. Ghosez, J.-Y. Raty, and D. C. Allan, Comput. Mater. Sci. **25**, 478 (2002); X. Gonze, G.-M. Rignanese, M. Verstraete, J.-M. Beuken, Y. Pouillon, R. Caracas, F. Jollet, M. Torrent, G. Zerah, M. Mikami, Ph. Ghosez, M. Veithen, J.-Y. Raty, V. Olevano, F. Bruneval, L. Reining, R. Godby, G. Onida, D. R. Hamann, and D. C. Allan, Z. Kristallogr. **220**, 558 (2005).

[18]J. P. Perdew, K. Burke, and M. Ernzerhof, Phys. Rev. Lett. **77**, 3865 (1996).

[19]M. Torrent, F. Jollet, F. Bottin, G. Zerah, and X. Gonze, Comput. Mater. Sci. **42**, 337 (2008).

[20]L. V. Pourovskii, K. Delaney, C. G. Van de Walle, N. A. Spaldin, and A. Georges, Phys. Rev. Lett. **102**, 096401 (2009).

[21]P. Pellegrino, B. Garrido, J. Arbiol, C. Garcia, Y. Labour, and J. R. Morante, Appl. Phys. Lett. **88**, 121915 (2006).

[22]A. Ziegler, J. C. Idrobo, M. K. Cinibulk, C. Kisielowski, N. D. Browning, and R. O. Ritchie, Science **306**, 1768 (2004).

[23]C. C. Ahn and O. L. Krivanek, *EELS Atlas: A Reference Guide of Electron Energy Loss Spectra Covering All Stable Elements* (Gatan, Warrendale, 1983).

[24]S. Sato, S. Nozaki, and H. Morisaki, Thin Solid Films **343–344**, 481 (1999).

[25]R. Pantel, M. C. Cheynet, and F. D. Tichelaar, Micron **37**, 657 (2006).

[26]E. Bertel, F. P. Netzer, and J. A. D. Matthew, Surf. Sci. **103**, 1 (1981).

[27]R. F. Loane, E. J. Kirkland, and J. Silcox, Acta Crystallogr. Sect. A **44**, 912 (1988).